

## Supporting Information

### Reversible Cl/Cl<sup>-</sup> Redox in a Spinel Mn<sub>3</sub>O<sub>4</sub> Electrode

Sean K. Sandstrom,<sup>#a</sup> Qiuyao Li,<sup>#b</sup> Yiming Sui,<sup>#a</sup> Mason Lyons,<sup>c</sup> Chun-Wai Chang,<sup>c</sup> Rui Zhang,<sup>d</sup> Heng Jiang,<sup>a</sup> Mingliang Yu,<sup>a</sup> David Hoang,<sup>a</sup> William F. Stickle,<sup>c</sup> Huolin L. Xin,<sup>\*d</sup> Zhenxing Feng,<sup>\*c</sup> De-en Jiang<sup>\*bf</sup> and Xiulei Ji<sup>\*a</sup>

---

a. Department of Chemistry, Oregon State University, Corvallis, OR, 97331, USA.

b. Interdisciplinary Materials Science Program, Vanderbilt University, Nashville, TN, 37235, USA.

c. School of Chemical, Biological, and Environmental Engineering, Corvallis, OR, 97331, USA.

d. Department of Physics and Astronomy, University of California, Irvine, CA, 92697, USA.

e. Hewlett-Packard Co., Corvallis, OR, 97330, USA.

f. Department of Chemical and Biomolecular Engineering, Vanderbilt University, Nashville, TN, 37235, USA.

Emails: [david.ji@oregonstate.edu](mailto:david.ji@oregonstate.edu), [de-en.jiang@vanderbilt.edu](mailto:de-en.jiang@vanderbilt.edu), [zhenxing.feng@oregonstate.edu](mailto:zhenxing.feng@oregonstate.edu)  
[huolin.xin@uci.edu](mailto:huolin.xin@uci.edu)

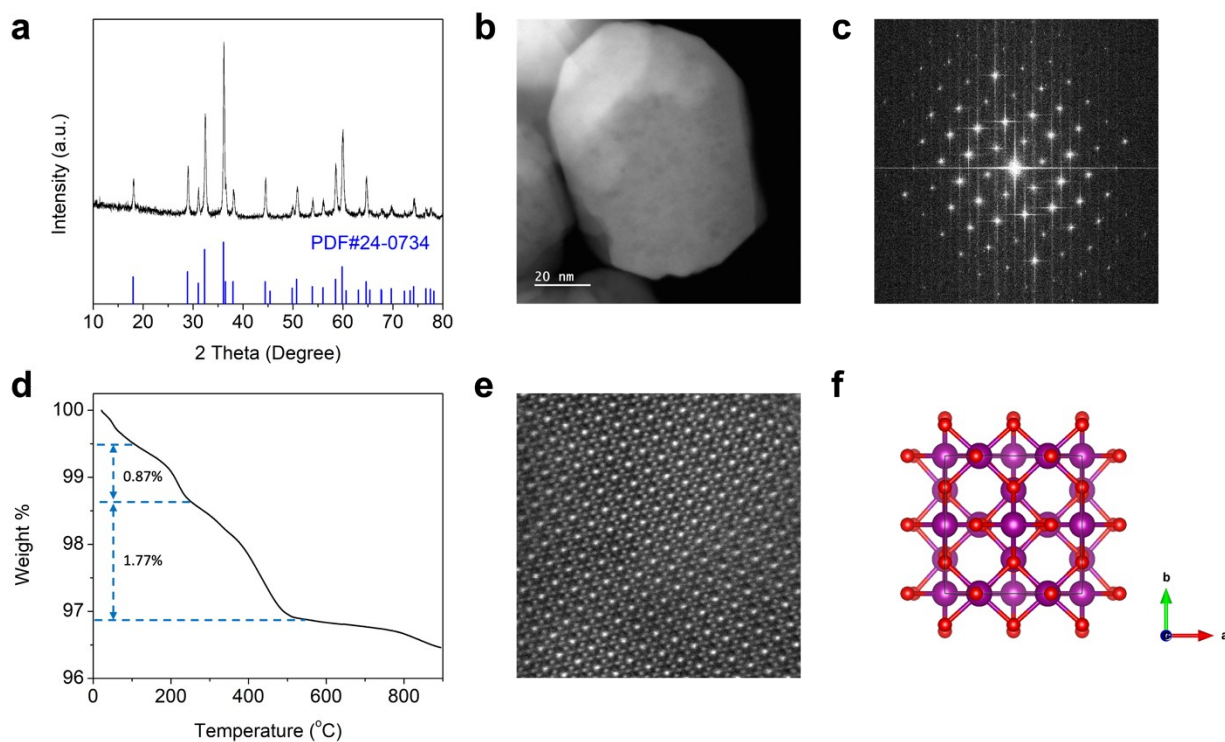


**Figure S1.** Material characterization of the as synthesized  $\text{Mn}_3\text{O}_4$ . (a) XRD pattern of the  $\text{Mn}_3\text{O}_4$  powder. (b) STEM image of a representative  $\text{Mn}_3\text{O}_4$  particle and (c) the associated electron diffraction pattern. (d) TGA curve of the  $\text{Mn}_3\text{O}_4$  powder obtained under argon atmosphere at a ramp rate of  $10\text{ }^\circ\text{C}/\text{min}$ . (e) STEM image and (f) an ideal spinel crystal structure of the as synthesized  $\text{Mn}_3\text{O}_4$  powder.

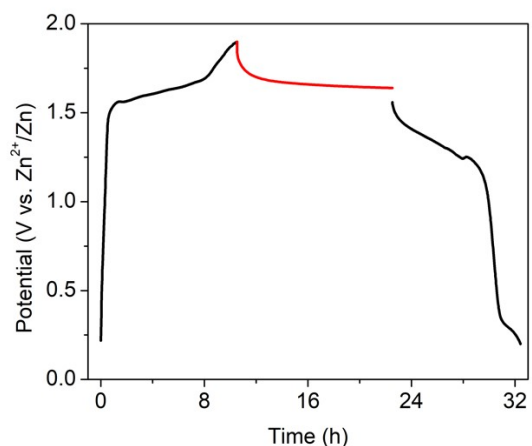


**Figure S2.** Self-discharge performance of the  $\text{Zn}^{2+}$ -trapped  $\text{Mn}_3\text{O}_4$  electrode after being charged in the 20 *m*  $\text{ZnCl}_2$  + 5 *m*  $\text{NH}_4\text{Cl}$  WiSE. The red portion of the curve shows the self-discharge behavior while resting the cell for 12 hours. Cycling was done using a  $\text{Mn}_3\text{O}_4$  free-standing film electrode at 100 mA/g. The Coulombic efficiency after idling the cell was 94.3%.

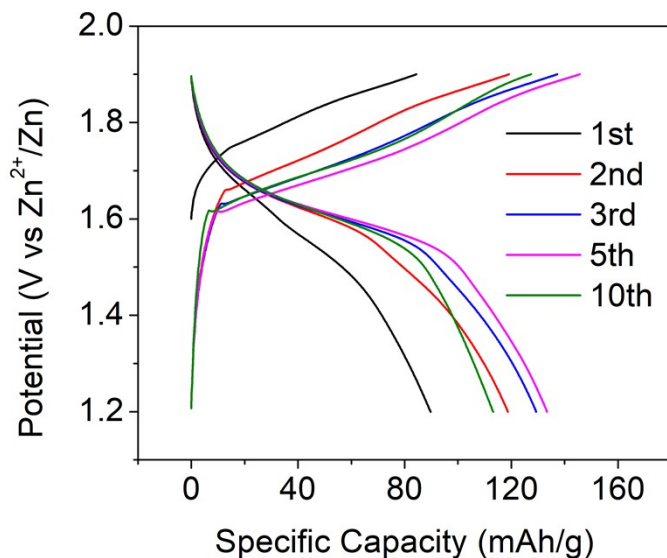


**Figure S3.** GCD profiles of the first, second, third, fifth, and tenth cycles of the  $\text{Mn}_3\text{O}_4$  electrode without initially trapping  $\text{Zn}^{2+}$  ions (charging first and increasing the lower cutoff potential to 1.2 V) at a current rate of 50 mA/g.

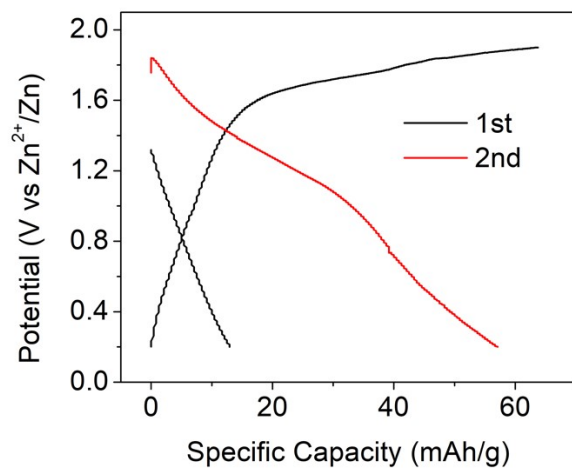


**Figure S4.** GCD profiles of the  $\text{Mn}_3\text{O}_4$  electrode obtained at 50 mA/g using 15 *m* TEACl as the aqueous electrolyte. Activated carbon was used as the counter electrode and Ag/AgCl was used as the reference electrode. Reference potentials were converted to being vs  $\text{Zn}^{2+}/\text{Zn}$  for comparison.

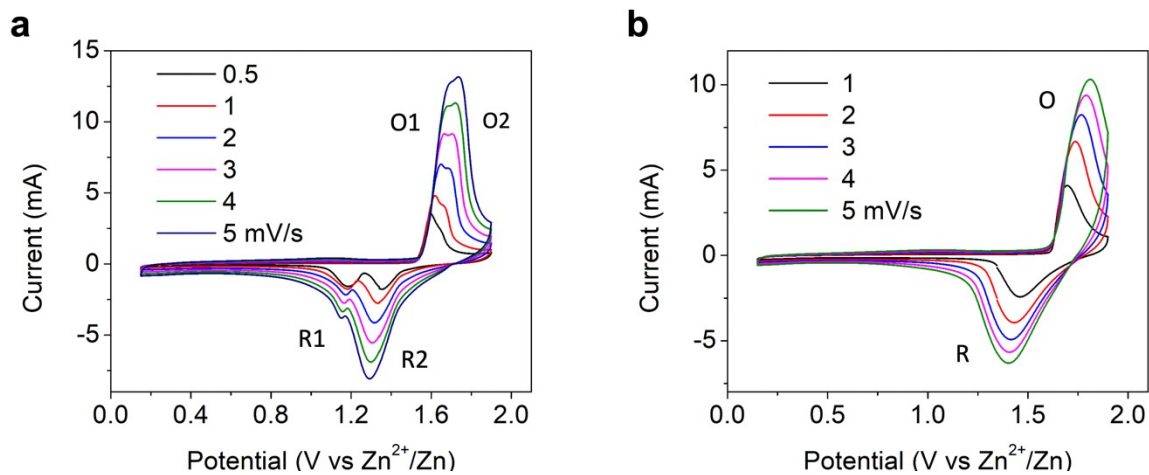


**Figure S5.** CV curves of the  $\text{Mn}_3\text{O}_4$  electrode in (a) 2 M  $\text{ZnSO}_4$  and (b) 20 *m*  $\text{ZnCl}_2$  + 5 *m*  $\text{NH}_4\text{Cl}$  electrolytes at a scan rate of 1 mV/s.

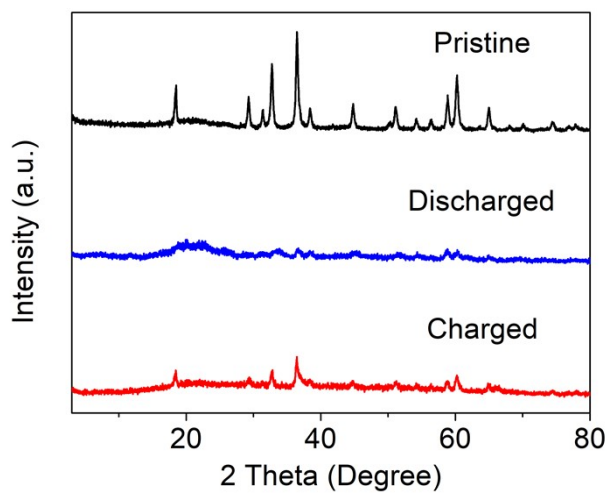


**Figure S6.** XRD patterns of the pristine, discharged, and charged  $\text{Mn}_3\text{O}_4$  electrodes in the WiSE.

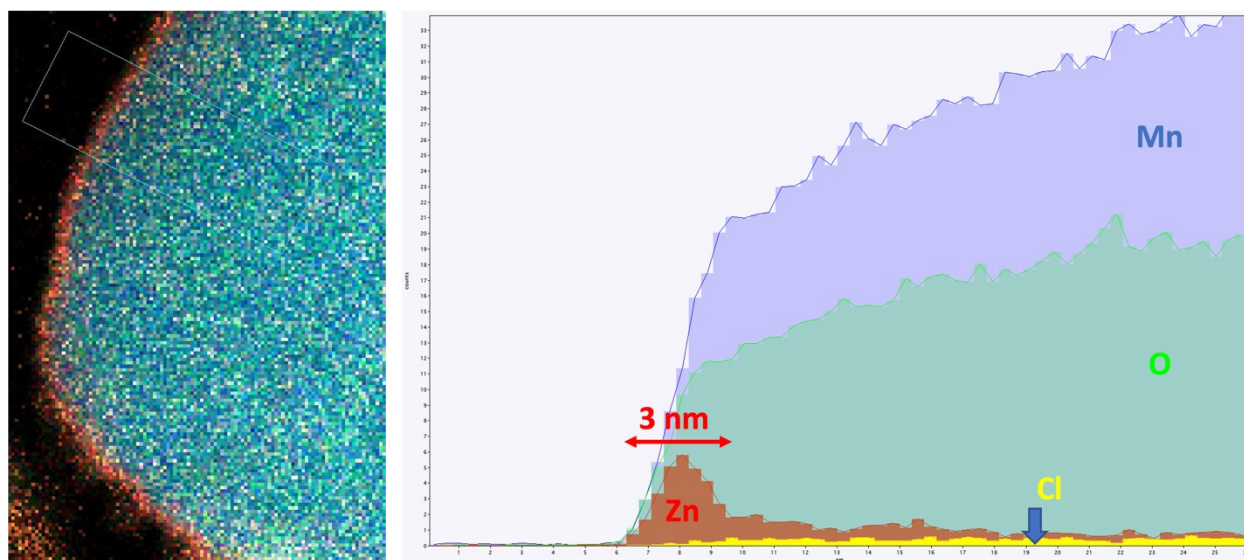


**Figure S7.** EDS line scanning profile of the  $\text{Mn}_3\text{O}_4$  electrode after the first charge. The Mn, O, and Cl contents are distributed fairly uniform throughout the particle, whereas the Zn content is concentrated toward the outer 3 nm of the particle.

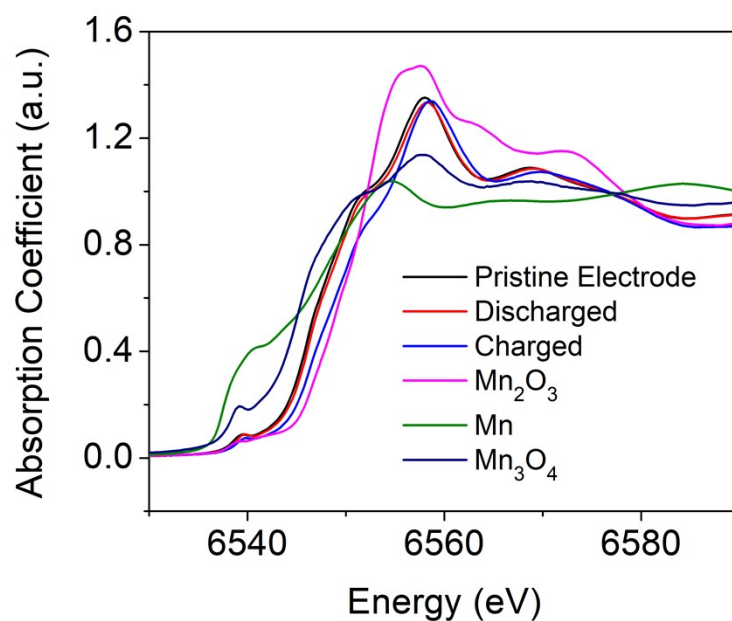


**Figure S8.** Normalized XANES of the Mn K-edge spectra of the pristine Mn<sub>3</sub>O<sub>4</sub> electrode, the Mn<sub>3</sub>O<sub>4</sub> electrode after the first discharge and the first charge in the 20 *m* ZnCl<sub>2</sub> + 5 *m* NH<sub>4</sub>Cl WiSE, and the Mn<sub>2</sub>O<sub>3</sub>, Mn<sub>3</sub>O<sub>4</sub>, and Mn metal standards. The similar edge positions between the pristine, discharged, and charged samples highlight the lack of significant Mn redox after cycling the electrode.

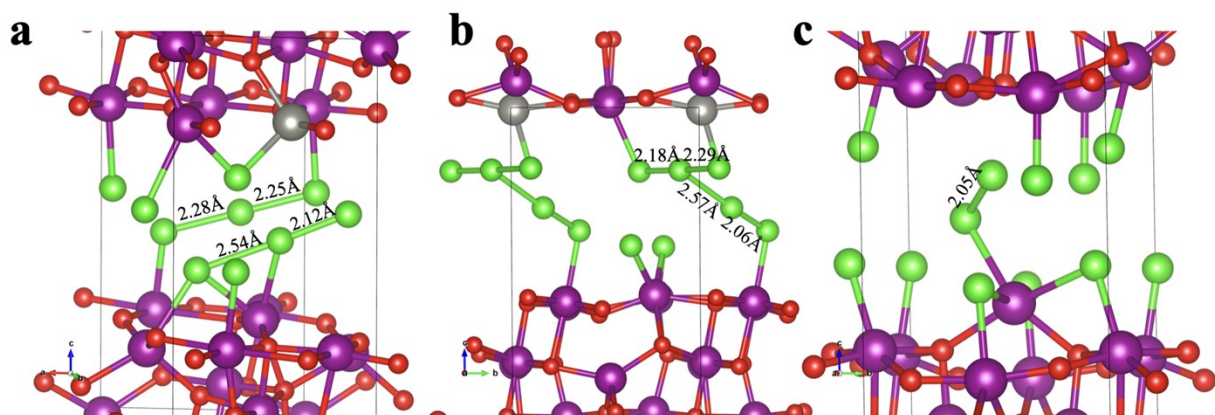


**Figure S9.** Zoomed-in images of Cl inserted in Mn<sub>3</sub>O<sub>4</sub> structure with Zn-trapped in (a) octahedral site, (b) tetrahedral site, and (c) pristine Mn<sub>3</sub>O<sub>4</sub> structure without Zn-trapped. The formation of trichloride [Cl<sub>3</sub>]<sup>-</sup> in ZnOh, T-shaped pentachloride [Cl<sub>5</sub>]<sup>-</sup> in ZnTd, and dichloride in Mn<sub>3</sub>O<sub>4</sub> with corresponding bond distances between Cl atoms are shown in the figure.

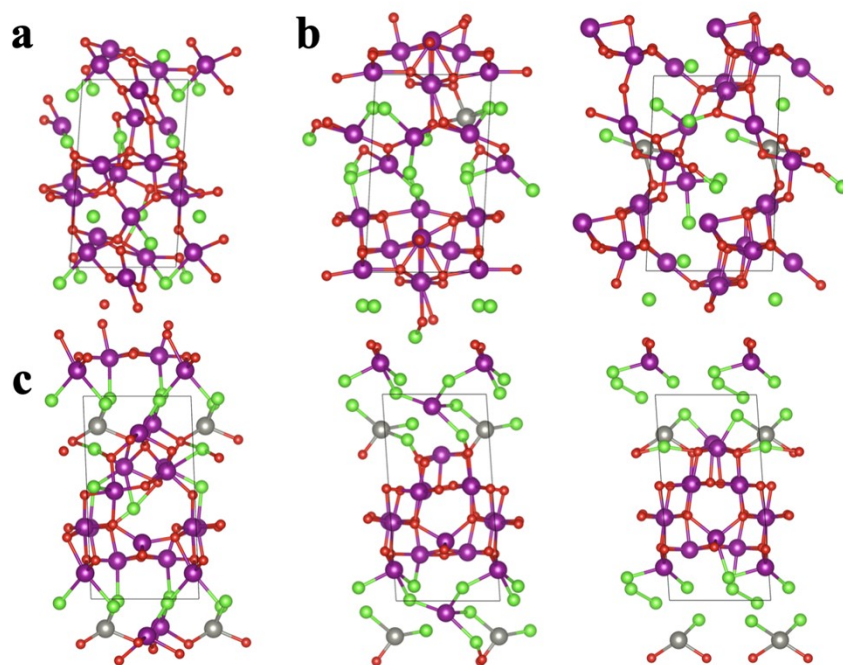


**Figure S10.** Possible optimized structures of Cl intercalation in (a) pristine Mn<sub>3</sub>O<sub>4</sub>, (b) ZnOh, and (c) ZnTd.

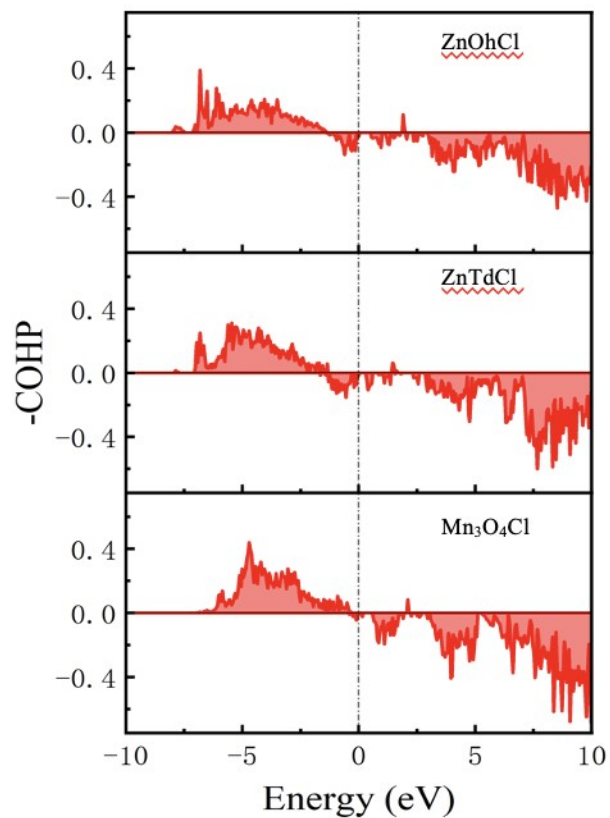


**Figure S11.** COHP analysis of Mn-Cl bond after Cl insertion in (a) ZnOh, (b) ZnTd, and (c)  $\text{Mn}_3\text{O}_4$  models.

**Table S1.** Calculated Zn insertion energies of ZnOh, and ZnTd.

	ZnOh	ZnTd
<b>Zn insertion energy (eV)</b>	-0.86	-0.98

**Table S2.** Bader charge analysis of Mn, O, Zn, and Cl before and after Cl/Cl<sup>-</sup> insertion in the pristine Mn<sub>3</sub>O<sub>4</sub>, the octahedral site Zn-trapped Mn<sub>3</sub>O<sub>4</sub>, and the tetrahedral site Zn-trapped Mn<sub>3</sub>O<sub>4</sub>.

<b>Average Bader charge</b>	<b>Mn</b>	<b>O</b>	<b>Zn</b>	<b>Cl</b>
Mn <sub>3</sub> O <sub>4</sub>	1.57	-1.17	-	-
ZnOh	1.52	-1.21	1.16	-
ZnTd	1.51	-1.21	1.17	-
Mn <sub>3</sub> O <sub>4</sub> (after Cl insertion)	1.62	-1.06	-	-0.34
ZnOh (after Cl insertion)	1.56	-1.13	1.18	-0.27
ZnTd (after Cl insertion)	1.57	-1.14	1.18	-0.26